Surface Depletion Induced Quantum Confinement in CdS Nanobelts

Dehui Li,[†] Jun Zhang,[†] and Qihua Xiong[†,‡,*]

[†]Division of Physics and Applied Physics, School of Physical and Mathematical Sciences, Nanyang Technological University, Singapore 637371 and
[‡]Division of Microelectronics, School of Electrical and Electronic Engineering, Nanyang Technological University, Singapore 639798

ABSTRACT

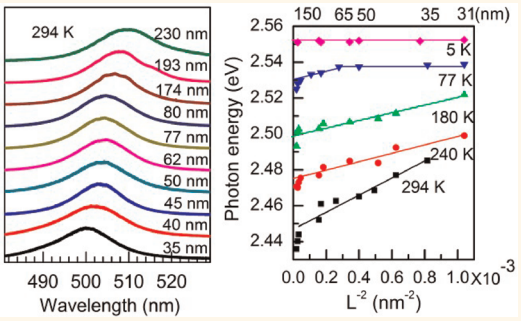

We investigate the surface depletion induced quantum confinement in CdS nanobelts beyond the quantum confinement regime, where the thickness is much larger than the bulk exciton Bohr radius. From room temperature to 77 K, the emission energy of free exciton A scales linearly *versus* $1/L^2$ when the thickness L is less than 100 nm, while a deviation occurs for those belts thicker than 100 nm due to the reabsorption effect. The $1/L^2$ dependence can be explained by the surface depletion induced quantum confinement, which modifies the confinement potential leading to a quasi-square potential well smaller than the geometric thickness of nanobelts, giving rise to the confinement effect to exciton emission beyond the quantum confinement regime. The surface depletion is sensitive to carrier concentration and surface states. As the temperature decreases, the decrease of the electrostatic potential drop in the surface depletion region leads to a weaker confinement due to the decrease of carrier concentration. With a layer of polymethyl methacrylate (PMMA) passivation, PL spectra exhibit pronounced red shifts due to the decrease of the surface states at room temperature. No shift is found at 10 K both with or without PMMA passivation, suggesting a much weaker depletion field due to the freezing-out of donors.

KEYWORDS: CdS nanobelts · quantum confinement · surface depletion · photoluminescence · surface passivation · reabsorption

In the past decade, zero- and one-dimensional semiconductor nanomaterials and heterostructures (quantum dots, nanowires, or nanobelts) have attracted tremendous attention due to their unprecedented properties derived from their quantum size in at least one dimension or strong anisotropy (*e.g.*, antenna effect in 1D cases).[1−3] When the physical dimension of nanomaterials (for instance, diameter of quantum dots or nanowires and thickness of nanobelts) becomes comparable to or smaller than the characteristic lengths of elemental excitations, such as the mean free path of electron or phonon and the Bohr radius of exciton, at finite temperature, a quantum confinement effect is anticipated, giving rise to the blue shift of the band gap in terms of electronic states[4] and the red shift of confined phonon states.[3,5] One particular exciting achievement in direct band gap semiconductor quantum dots and nanowires is the tunable emission based on quantum confinement.[6−9] It is generally believed that the bulk exciton Bohr radius (a_B) is the approximate dimension for the onset of the quantum confinement effect.[2] However, the blue shift of the band gap *versus* size parameter has also been observed in CdS[10] and WSe_2 slabs,[11] CdSe[12] and InP nanowires,[13] ZnO nanowires,[14] and nanopencils[15] beyond the quantum confinement regime, *i.e.*, when the size parameter is larger than a_B. For instance, Buhro *et al.* investigated the transition from 3D to 2D confinement in CdSe nanorods and found that the minimum length of the nanorods exhibiting 2D confinement is as large as 30 nm, 6 times larger than a_B (~5 nm).[4] The blue shift of the photoluminescence (PL) peak compared to their bulk counterpart was also found in InP nanowires with a diameter of 50 nm ($a_B \approx 19$ nm).[13] Although surface emission[14] and the Burstein−Moss (BM) effect have been proposed to explain the anomalous blue shift of the emission spectra of nanowires and nanobelts with a size far beyond the quantum confinement regime,[12,15] the underlying physical mechanism is still not well understood, and further investigations are demanded.

One-dimensional nanowires and nanobelts have attracted a great deal of interest owing to their potential applications in lasers,[16,17] waveguides,[18,19] LEDs,[20,21] and photodetectors[22−25] and their interesting fundamental physical properties.[26−29] CdS is a direct wide band gap (2.54 eV) compound semiconductor with an exciton binding energy[30] of 28 meV and a a_B of 3.2 nm.[10]

* Address correspondence to Qihua@ntu.edu.sg.

Received for review March 9, 2012 and accepted May 11, 2012.

Published online May 11, 2012
10.1021/nn301053r

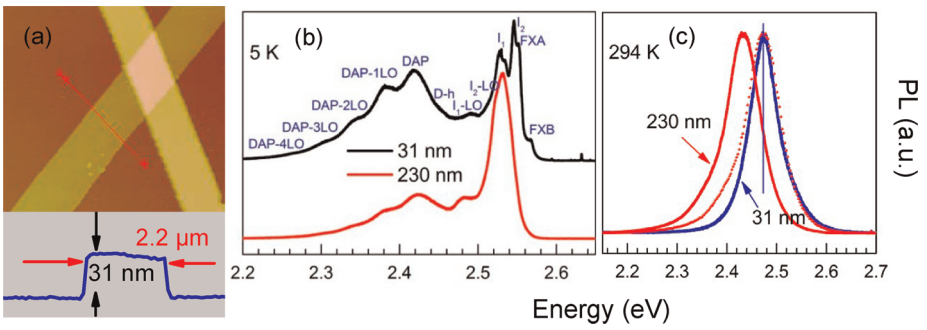

Figure 1. (a) AFM image: the top frame is the topography image, while the bottom frame is the section profile along the red lines shown in the topography image. The nanobelt shown here is 31 nm thick, and the thicker stripe at the right side is the Ti/Au electrode used for photoconductivity measurements. The PL spectra of a 31 nm and a 230 nm CdS nanobelt at 5 K (b) and 294 K (c). The peak assignments are labeled in (b). In (c), the spectrum of the 230 nm belt is shifted to the higher energy side by 40 meV, shown as the dotted red line in order to compare the line shape.

CdS nanowires and nanobelts have been demonstrated to have potential applications in nano-optoelectronic devices,[31,32] such as visible range photodetection,[24,33,7] electro-absorption modulators,[34,35] and laser devices.[16] In terms of nano-optoelectronic applications, a profound understanding of the influence of nanoscale size on the emission properties beyond the quantum confinement regime is essential for the device optimization and integration.

In this report, we have investigated how the PL peaks evolve with the thickness of the CdS nanobelts beyond the quantum confinement region and elucidate the physical mechanism using temperature- and power-dependent PL spectroscopy supported by photoconductivity measurements. At 77 K and above, the PL peaks show a systematic blue shift as the thickness of the nanobelt decreases. The emission peak energy *versus* the thickness can be well fitted with an inverse square function. Below 77 K, no apparent shift of the emission peaks is present. The thickness dependence of emission energy beyond the quantum confinement regime is explained by the surface depletion induced quantum confinement. Finally, PL measurements of the CdS nanobelts covered with a layer of polymethyl methacrylate (PMMA) have been conducted to verify the surface depletion induced quantum confinement.

RESULTS AND DISCUSSION

A typical atomic force microscopy (AFM, Veeco Instrument, Nanoscope III) image for a 31 nm nanobelt is shown in Figure 1a. The nanobelt is observed to exhibit uniform thickness and width. The typical PL spectra of 31 and 230 nm nanobelts at 5 K are shown in Figure 1b. The absence of surface state related emission and rich distinct exciton emission-related features indicate the high crystalline quality of our samples. According to the PL spectrum of the ensemble CdS nanobelts,[36,37] the emission peaks can be assigned as labeled in Figure 1b. Due to the crystal field and spin−orbit interactions, the valence band splits into three bands. The corresponding excitons are labeled as free exciton A (FXA), free exciton B (FXB), and free exciton C (FXC) with characteristic energies of 2.550, 2.568, and 2.629 eV, respectively.[38] Therefore, the peaks at 2.568 and 2.552 eV can be assigned as FXB and FXA. Other peaks can be assigned to neutral donor bound exciton emission (I_2), neutral acceptor bound exciton emission (I_1), first-order phonon replica of I_2 and I_1, hole bound to donor emission (D-h), donor−acceptor pair emission (DAP), and phonon replica of DAP, respectively, as we previously discussed involving cadmium and sulfur vacancies.[36]

The FXA and FXB peaks can be clearly distinguished in the 31 nm belt, while they are smeared into one broad peak in the 230 nm belt. This smearing in the 230 nm nanobelt is probably due to the presence of reabsorption in the thick belts. When the thickness of the nanobelts is larger than half of the wavelength of the emitted light in the nanobelts, the emitted light could be trapped inside the belt due to the internal reflection and be absorbed again. For CdS, the wavelength of the emitted light in the nanobelts will be ~200 nm at room temperature if we take the emission peak as 500 nm and the refractive index as 2.5 at 500 nm.[30] The reabsorption would lead to a red shift, a broadening of the emission peak, and a long tail at the longer wavelength side at higher temperatures.[19,39,40] As the temperature decreases, the narrowing of the thermal broadening gradually diminishes the red shift.[39] However, the reabsorption can still give rise to peak broadening at 5 K, which makes the free exciton emission peaks unresolvable in the 230 nm belt (Figure 1b).

The reabsorption effect in the 230 nm belt is further demonstrated by the line shape of the room-temperature PL spectra, as shown in Figure 1c. In order to compare the line shape between these two spectra, the spectrum of the 230 nm nanobelt has been shifted horizontally toward the higher energy side by 40 meV, shown as a dotted curve in Figure 1c. In contrast to the symmetric line shape of the PL spectrum of the 31 nm nanobelt, the asymmetric line shape of the PL spectrum of the 230 nm nanobelt with a long tail at the

longer wavelength side confirms the presence of the reabsorption.

The thickness (L)-dependent PL spectra at 294, 240, and 180 K are shown in Figure 2a–c. As the thickness decreases, the emission peak continuously blue shifts and the line shape of the emission peak gradually evolves from asymmetric with a long tail at the lower energy side to symmetric at a thickness less than 100 nm. At 77 K, for the belts with a thickness larger than 60 nm, only one broad peak can be resolved, which shows a slight blue shift as the thickness decreases, as shown in Figure 2d. Strikingly, two distinct peaks appear in the thinner belts, as shown noticeably for thicknesses of 50, 40, and 31 nm at 77 K. A negligible shift of those two distinct peaks is observed for L less than 60 nm (Figure 2e). When the samples are further cooled to 5 K, no peak shift of the corresponding excitons among the different thickness belts is exhibited, as shown in Figure 2f. The free exciton and bound exciton emission peaks show a narrow line shape in the thin belts. As a result, these peaks are well separated from each other. However, due to the large line width of those peaks in the thicker belts, they are smeared into a broad peak (*e.g.*, 80 and 230 nm).

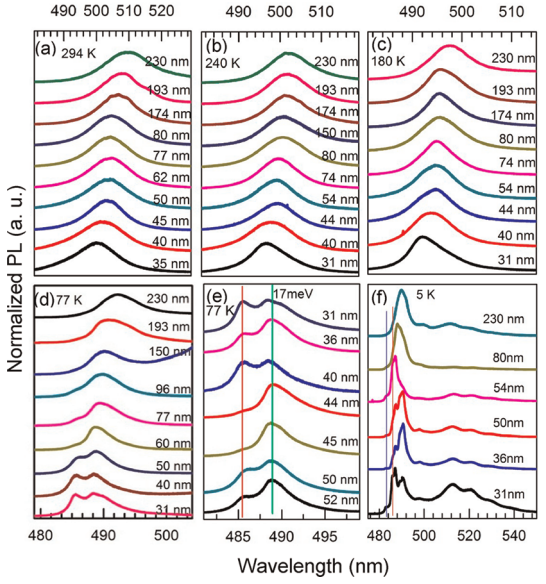

Figure 2. PL spectra of belts with various thickness at 294K (a), 240 K (b), 180 K (c), 77 K (d), and 5 K (f). (e) PL spectra of nanobelts with a thickness less than 60 nm at 77 K. All spectra are offset vertically for clarity.

On the basis of the Voigt function fitting, the energies of FXA and FXB emission peaks can be extracted. The energy of the FXA emission peak is plotted *versus* $1/L^2$ at various temperatures in Figure 3a. The following information can be extracted from Figure 3a: (1) at 77 K and above, the FXA emission peak scales linearly with $1/L^2$ up to a thickness of 100 nm. The intercept at the vertical axis corresponds to the FXA emission energy in the bulk (*i.e.*, when L approaches infinity). We can define a quantity of energy shift $\Delta E = E(L) - E(L \rightarrow \infty)$. When the thickness is 31 nm, we can obtain a maximum energy shift ΔE of 38 meV at 294 K, 24 meV at 240 K, 18 meV at 180 K, and 8 meV at 77 K, respectively. The FXA emission is no longer dependent on thickness at 5 K. (2) When the thickness L is more than 100 nm, the energy shift ΔE deviates from a linear dependence on $1/L^2$. The deviation becomes smaller and smaller as the temperature decreases and completely disappears at 5 K. (3) At 77 K, the FXA emission peak also exhibits linearly shifting with $1/L^2$ for the thickness L ranging from 60 to 100 nm, but no shift is observed when L is less than 60 nm. The maximum energy shift is around 8 meV, much smaller than that obtained at 294 K.

The extracted FXA energy in the bulk, $E(L \rightarrow \infty)$, *versus* temperature is plotted in Figure 3b. The energy of the FXA emission peak shows a red shift as the temperature increases due to the enhanced electron–phonon interaction and the lattice expansion. The energy of FXA as a function of temperature can be described by the empirical Varshni equation:[37] $E(T) = E(0) - \alpha T^2/(T + \beta)$, where $E(0)$ is the energy of FXA at 0 K and α and β are constants related to the certain materials. Our result can be well fitted by the Varshni equation, with fitting parameters $E(0) = 2.550 \pm 0.002$ eV, $\alpha = 0.38 \pm 0.04$ meV K^{-1}, and $\beta = 43 \pm 30$ K, in good agreement with the previous reports.[37,38]

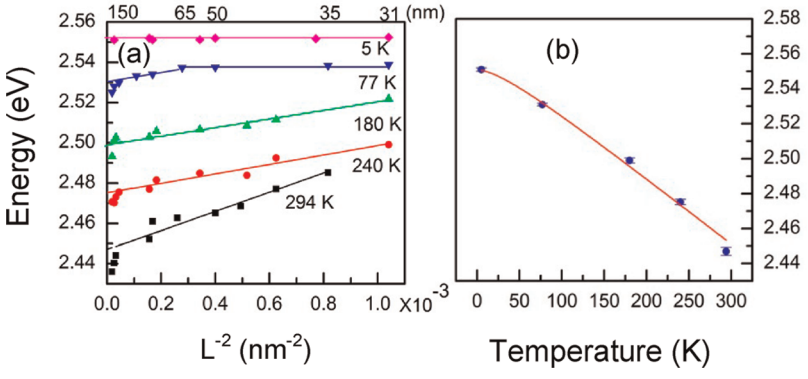

Figure 3. (a) Photon energy of FXA emission *versus* the thickness of nanobelts at various temperatures. (b) Extrapolating the linear fitting of (a) to infinite thickness, the energy of FXA in the bulk can be extracted. The extrapolated photon energy of FXA is plotted against temperature. The dots represent the extrapolated data, and the solid line is the Varshni fitting.

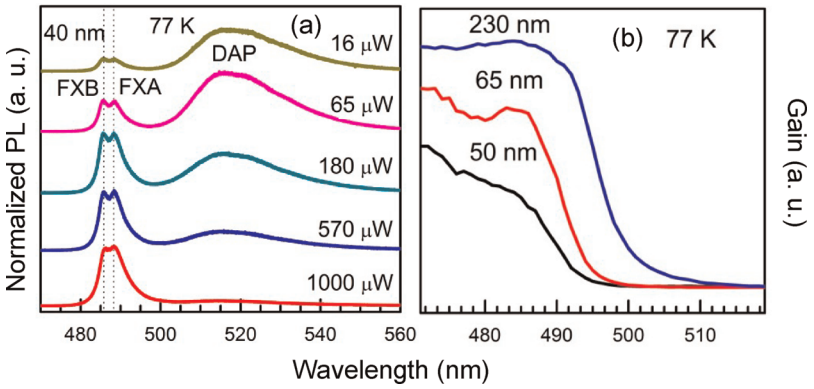

Figure 4. (a) Power dependence of PL spectra of a 40 nm belt at 77 K excited by a 457 nm laser. The vertical dot lines indicate the positions of FXA and FXB emission. The broad peak at the longer wavelength side is DAP emission. The spectra are vertically offset for clarity. (b) Photoconductivity gain spectra of 50, 65, and 230 nm CdS nanobelts at 77 K.

The deviation from the linear $1/L^2$ dependence of FXA emission energy for those belts with a thickness more than 100 nm can be ascribed to the reabsorption as mentioned previously. The reabsorption leads to a red shift of the emission peak. Because the thermal broadening is reduced as the temperature decreases, the deviation becomes smaller and smaller and completely disappears at 5 K.[39]

The blue shift of the PL emission peaks has been observed both in the quantum confinement regime ($l \approx a_B$, where l is the characteristic length in the confinement direction) and beyond the quantum confinement regime ($l \gg a_B$). In the strong quantum confinement regime ($l < a_B$), the quantum confinement originates from the geometric confinements of electrons and holes as independent particles.[41] The small geometric size l deforms the wave functions of electrons and holes, leading to an increase of the band gap and the exciton binding energy.[2] The particle-in-a-box model has been used most frequently to describe the confinement effect: $\Delta E = \hbar^2\pi^2/2\mu l^2$, where $\hbar$ is the Planck constant and $\mu = m_e m_h/(m_e + m_h)$ is the reduced mass of electron and hole. m_e and m_h are the effective mass of the electron and hole, respectively. Experimental reports in the strong confinement regime have proved the linear $1/l^2$ dependence of the band gap shift proposed by the particle-in-a-box model.[9] Deviation from linear $1/l^2$ dependence has also been observed. For instance, the band gap energy scales linearly *versus* $1/l^{1.36}$ in CdSe nanowires[4] and $1/l^{1.46}$ in InP nanowires.[42] In the weak confinement region ($l > a_B$), the confinements on electrons and holes are small and the Coulomb interaction is dominant. As a consequence, there occurs a size quantization of the motion of the exciton in the confinement dimensions.[41] By applying the particle-in-a-box model, the shift of band gap energy follows the linear $1/l^2$ as well, but with a different energy shift ($\Delta E = \hbar^2\pi^2/2Ml^2$, where $M = m_e + m_h$ is the mass of the exciton). The peak shift of exciton emission caused by the quantization of the motion of the exciton has been observed in CdS slabs.[10] Beyond the quantum confinement regime ($l \gg a_B$), the band gap energy also shows an anomalous blue shift as the size decreases. Recently, Yu *et al.*[12] reported that the blue shift of the emission peak exhibits $1/l^{2/3}$ dependence in the CdSe nanowires with diameters ranging from 50 to 700 nm. They attributed this blue shift to the BM effect due to high carrier concentration induced by surface vacancies and laser excitation.

Our results can be explained by neither exciton confinement nor BM effect. Taking a 31 nm belt at 294 K as an example to do a rough estimation, using $m_e = 0.2m_0$ and $m_h = 1.35m_0$ (m_0 is the mass of electron),[43] the energy shift ΔE is 2.23 meV for the confinement of the electron and hole and 0.25 meV for the confinement of the exciton, while our experimental energy shift of the 31 nm belt is 38 meV, much larger than either of the calculated values. In addition, the temperature dependence of the energy shift ΔE cannot be explained by the particle-in-a-box model, unless the confinement length l is able to change with the temperature because the effective masses of both electron and hole are insensitive to the temperature, supported by parabolic band approximation.

Furthermore, the BM effect induced by laser excitation is not applicable to our experimental results. The BM effect is an important phenomenon in degenerate semiconductors, which causes the blue shift of the optical gap in the absorption and photoluminescence spectra.[44] Taking an n-type degenerate semiconductor as an example, the Fermi level is positioned inside the conduction band due to the filling of the conduction band by electrons. As such, the absorption can be contributed only by the optical transition between the valence band and the unoccupied conduction band above the Fermi level, which gives rise to the apparent increasing of the optical gap. Therefore, the BM shift would increase with the excitation power, as a higher excitation power increases electron concentration. The excitation power-dependent PL spectra of a 40 nm CdS belt at 77 K are given in Figure 4a. The two

vertical dashed lines indicate the positions of FXA and FXB emission, and the broad band at the longer wavelength side is the DAP emission. With the increase of the excitation power, the DAP emission saturates, suggesting that the cadmium vacancy levels become fully populated.[36] However, no noticeable shifts of FXA and FXB emission peaks are observed by varying the excitation power from 16 μW to 1 mW, which suggests that the carrier concentration is not high enough to give rise to the BM effect at those excitation powers. The excitation power used in Figure 2 falls into this range. In addtion, as the thickness decreases, the blue shift of the exciton peaks has also been observed in the photoconductivity spectra of individual CdS nanobelt devices both at room temperature[34] and at 77 K, as shown in Figure 4b. Detailed information about the photoconductivity measurements can be found elsewhere.[34] The photon excitation in photoconductivity measurements is provided by a tungsten halogen lamp, whose intensity magnitude is 5 orders smaller than the laser power intensity used here for PL studies. This is additional strong evidence that the BM effect cannot explain the thickness dependence of the anomalous blue shift in our samples.

The linear $1/L^2$ dependence of the FXA emission energy in CdS nanobelts can be ascribed to the surface depletion induced quantum confinement effect. The surface depletion induced quantum confinement can occur only in the thickness direction because of the much larger size in the width and length direction. The breaking of the translational symmetry of the crystal potential at the semiconductor surface leads to the formation of the surface states within the gap near the surface.[45] The distribution of the surface states forms a continuum within the band gap. A neutral level ϕ_0 is introduced to characterize this continuum, as shown in Figure 5. When the surface states are occupied up to the neutral level ϕ_0, the surface is electrically neutral. At thermodynamic equilibrium, electrons flow to the surface of an n-type semiconductor, thereby creating a layer of negative surface charge, which produces two depletion layers near both surfaces of the nanobelts, as shown in Figure 5a–c. The existence of the depletion regions effectively generates a modified potential well that confines carriers into a region smaller than the geometrical size of the structure, *e.g.*, thickness of the nanobelt.[46–48] The as-grown CdS nanobelts synthesized by the physical vapor transport method are usually n-type due to the sulfur vacancies.[24] According to a previous report,[49] the surface neutral level ϕ_0 lies 0.46 eV below the conduction band, which is much larger than the thermal energy (5–294 K). Therefore, it is reasonable for us to assume that the surface neutral level stays constant with the variation of the temperature.

The width of the depletion region d is related to the electrostatic potential drop V_d in the depletion region

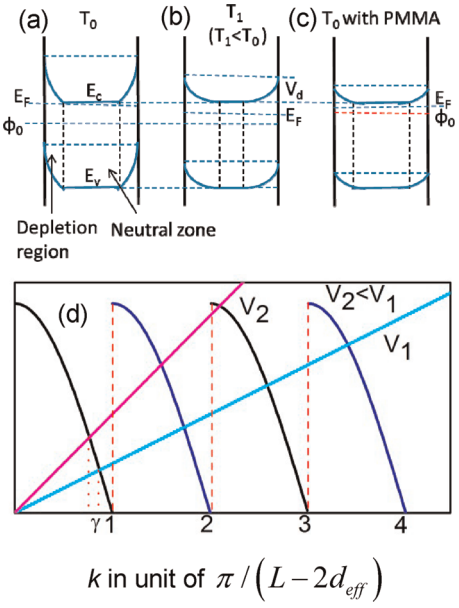

Figure 5. Schematic diagrams of the energy band of CdS nanobelts at a temperature T_0 (a), at a lower temperature T_1 (b), and after surface passivation at T_0 (c). E_c and E_v represent the conduction band and the valence band, respectively. E_F is the Fermi level, and ϕ_0 is the neutral level. V_d is the electrostatic potential drop due to the surface depletion. (d) Graphical solutions of the finite square potential well. V_1 and V_2 are the height of the potential well. The eigenenergy is proportional to k^2.

and the electron concentration N_d by the expression[45]

$$d = \sqrt{\frac{2\varepsilon V_d}{eN_d}} \quad (1)$$

where ε is the dielectric constant, which is 8.87 for CdS,[43] and e is the elementary charge. The electrostatic potential drop V_d is the difference between the neutral level ϕ_0 at the surface and the Fermi level (E_F) inside the bulk. The Fermi level E_F will be lowered and the electron concentration N_d would also be decreased as the temperature T decreases.[50] Therefore, the width of the depletion region d is also a function of the temperature T. On the other hand, according to the charge neutrality, the depletion region d should increase due to the reduction of the electron concentration N_d at low tempertuare.

For an n-type semiconductor neglecting the acceptor concentration, the electron concentration is given by[51]

$$N_d = \sqrt{\frac{N_D N_C}{2}} \exp\left(\frac{E_C - E_D}{2k_B T}\right) \quad (2)$$

where N_D is the donor concentration, N_C is the effective density of states in the conduction band, E_D is the donor energy level, and k_B is Boltzmann's constant. The effective density of states in the conduction band N_C is around 2.28×10^{18} cm^{-3} at 300 K,[51] and $E_C - E_D$ is around 35 meV for CdS.[36]

We assume that the confinement potential is a finite square potential well with a depth of $V_d(T)$ and a width

of $L - 2d_{eff}(T)$. It should be noted that the effective width of the depletion region $d_{eff}(T)$ differs from the real width of the depletion region d but is somewhat related to d due to the finite square potential well approximation. This assumption is reasonable at temperatures higher than around 100 K, because the donors are nearly completely ionized, contributing to a high electron concentration,[51] which leads to the relatively narrow depletion region with a steep falling edge inside the structures (Figure 5a). For temperatures lower than around 100 K, part of the donors start to be frozen out, as predicted by expression 2. As a result, the electron concentration is greatly reduced, leading to the large depletion region and a gradual falling edge inside the structure (Figure 5b). The potential profile gradually changes approximately from a finite square potential well at high temperature ($T > 100$ K) to a parabolic potential well at low temperature ($T < 100$ K).[52] In a finite square potential well, no analytic solutions can be obtained. However, the graphical solutions can be obtained as shown in Figure 5d. The confinement eigenenergy is proportional to k^2, which is a function of both the depth $V_d(T)$ and width ($L - 2d_{eff}(T)$) of the well. In detail, the confinement energy is linear in $\gamma^2/[L - 2d_{eff}(T)]^2$, where γ is the analytical solution shown in Figure 5d. γ is a positive number always smaller than unity and is a function of $V_d(T)$, as given in Figure 5d.[53]

At a certain temperature, $d_{eff}(T)$ and γ are approximately the same for all nanobelts. Therefore, the energy shifts of PL peaks show $1/L^2$ dependence. Varying the temperature will change $d_{eff}(T)$ and γ, leading to a different energy shift ΔE. As the temperature is lowered, the electron concentration in the conduction band decreases, resulting in an increase of the depletion region width based on the charge neutrality (Figure 5b). However, the electrostatic potential drop V_d also decreases as the temperature decreases (Figure 5b). The decrease of the electrostatic potential drop would lead to a smaller γ, which further results in a smaller confinement energy, as shown in Figure 5d. As a consequence, the confinement becomes weaker, leading to the small energy shift ΔE at low temperature. Further cooling the samples to 5 K, most donors are frozen out. The electron concentration is so low that the depletion electric field is too weak to generate any confinement. As a result, no energy shift is observed for both FXA and FXB emission peaks (Figures 2f and 3a).

At 77 K, no energy shift for those belts with a thickness less than 60 nm (Figure 2e) indicates that those nanobelts have been completely depleted, which further suggests that the width of the depletion region d is around 30 nm at 77 K. Because the maximum energy shift ΔE is 8 meV, we can assume the electrostatic potential drop V_d is 8 mV. Substituting d and V_d into expression 1, electron concentration N_d can be estimated as $\sim 8.72 \times 10^{15}$ cm^{-3}. Applying

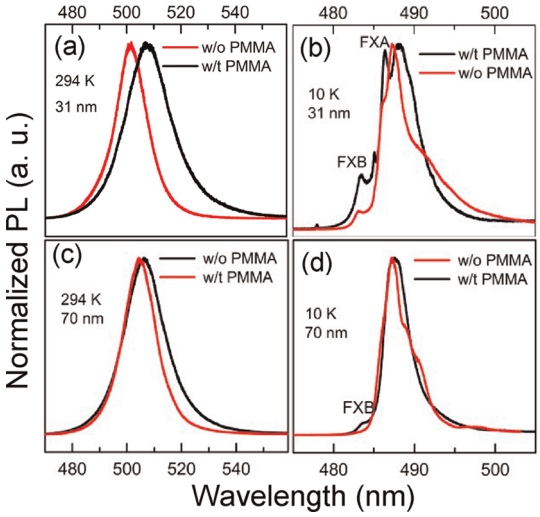

Figure 6. PL spectra of a 31 nm and a 70 nm belt with and without a layer of PMMA at 10 K (b and d) and 294 K (a and c).

$N_d = 8.72 \times 10^{15}$ cm^{-3} at 77 K to expression 2, the donor concentration $N_D = 8.36 \times 10^{16}$ cm^{-3} is obtained. This donor concentration is much lower than the critical electron concentration for BM effect to occur, which is around 2.1×10^{18} cm^{-3} for CdS according to the literature.[54] Therefore, quantitatively the BM effect cannot explain our experimental results either.

The surface depletion induced quantum confinement effect can be further examined by the surface passivation, which can greatly reduce the surface states. The reduction of the surface states leads to the narrowing of the depletion region d and the elevation of the neutral level ϕ_0 (Figure 5c).[55] The elevated neutral level ϕ_0 would further cause the reduction of the electrostatic potential drop V_d, as shown in Figure 5c. Both the narrowing of the depletion region and the reduction of the electrostatic potential drop would lead to the loss of the confinement strength at higher temperatures. Because the confinement energy follows the inverse square of the width of the confinement potential well, the reduction of the surface states exerts a much larger influence in the thin belts than that in the thick ones. At lower temperature, the depletion electric field is so weak that no confinement can be induced. The weak depletion electric field only broadens the emission peaks. The reduction of the depletion electric field leads to the decrease of the peak broadening (electric field broadening), which would give rise to the pronounced free exciton emission peaks after surface passivation.

The PL spectra of the belts covered with a layer of PMMA are shown in Figure 6. The emission peaks show red shifts after being passivated by a layer of PMMA at room temperature (Figure 6a and c). Compared with the 70 nm belt (Figure 6c), the red shift of the emission peaks is much larger in the 31 nm belt (Figure 6a), which demonstrates the loss of the confinement

strength after surface passivation, exactly as discussed previously. At 10 K, the free exciton emission is greatly enhanced for both the 31 nm and the 70 nm belts, as given in Figure 6b and d, suggesting the decrease of the electrical field induced peak broadening.

CONCLUSION

In conclusion, we have experimentally observed systematic blue shifts of the free exciton A emission of CdS nanobelts scaling linearly *versus* the inverse square of the belt thickness, which is much larger than the bulk exciton Bohr radius. Such a quantum confinement effect beyond the quantum confinement regime is attributed to surface depletion, which modifies the actual potential wells to be much smaller than the geometric nanobelt thickness and strongly depends on carrier concentration and surface states. This surface depletion thickness is found to be ~30 nm at 77 K. Surface depletion induced quantum confinement disappears at temperatures lower than 77 K due to donor freeze-out, while the surface passivation reduces surface states, leading to a loss of the confinement strength. The surface depletion induced quantum confinement may be responsible for the quantum-confined Stark effect[34] and may find applications in electro-absorption modulators and sensors.

METHODS

Nanobelt Synthesis. CdS nanobelts were synthesized in a home-built vapor transport chemical vapor deposition system, which is a very effective technique in growing one-dimensional structures from various compounds.[22,56,57] The detailed growth conditions, morphology, and crystalline characterizations can be found in our previous publications.[36,37] The CdS nanobelts are several micrometers in width, tens of micrometers in length, and 30−200 nm in thickness. The as-grown CdS nanobelts were dispersed into isopropyl alcohol solution and further deposited on a 500 nm SiO_2/Si substrate with prefabricated markers for the PL measurements on individual belts.

Photoluminescence Spectroscopy. The PL measurements of the individual CdS nanobelts were carried out under a Micro-Raman spectrometer (Horiba-JY T64000) in the backscattering configuration[58] excited by an Ar ion laser (457 nm) with a power intensity of 5 W/mm^2 (corresponding power: 400 μW).[34] A liquid helium continuous flow cryostat (Cryo Industry of America, USA) was used to provide a continuous temperature variation from 5 to 300 K. The PMMA was covered on the CdS nanobelts by spin-coating followed by a hard bake at 180 °C for 5 min.

Photoconductivity Spectroscopy. The PC measurements were performed using a home-built photoconductivity setup by using a two-probe FET configuration. The Ti/Au (60/50 nm) electrodes were patterned by electron beam lithography followed by thermal evaporation and a lift-off process. A quartz tungsten halogen lamp (250 W) was used as an excitation source, which was dispersed by a monochromator (Horiba JY HR320) with an energy resolution of 3 meV. The monochromatic light beam output was collimated and split into two beams: one was used to illuminate the devices mounted on the cryostat coldfinger, while the other was directed onto a pyroelectric detector (Newport, USA) to monitor the intensity of the incident light, in order to normalize the photon flux at different wavelengths. The photocurrent of a FET device and light intensity signals were both measured by two lock-in amplifiers (Stanford SR830) coupled with a mechanical chopper, which was used to modulate the incident light and to provide the reference signals to the lock-in amplifiers.

Conflict of Interest: The authors declare no competing financial interest.

Acknowledgment. Q.X. acknowledges strong support from Singapore National Research Foundation through a NRF fellowship grant (NRF-RF2009-06), start-up grant support (M58113004) and New Initiative Fund (M58110100) from Nanyang Technological University (NTU). Q.X. thanks Prof. R. Saito for his extremely helpful discussions.

REFERENCES AND NOTES

1. Chen, G.; Wu, J.; Lu, Q. J.; Gutierrez, H. R. H.; Xiong, Q. H.; Pellen, M. E.; Petko, J. S.; Werner, D. H.; Eklund, P. C. Optical Antenna Effect in Semiconducting Nanowires. *Nano Lett.* **2008**, *8*, 1341–1346.
2. Buhro, W. E.; Colvin, V. L. Semiconductor Nanocrystals: Shape Matters. *Nat. Mater.* **2003**, *2*, 138–139.
3. Adu, K. W.; Xiong, Q. H.; Gutierrez, H. R.; Chen, G.; Eklund, P. C. Raman Scattering As a Probe of Phonon Confinement and Surface Optical Modes in Semiconducting Nanowires. *Appl. Phys. A: Mater. Sci. Process.* **2006**, *85*, 287–297.
4. Yu, H.; Li, J.; Loomis, R. A.; Gibbons, P. C. Wang; Buhro, W. E. Cadmium Selenide Quantum Wires and the Transition from 3D to 2D Confinement. *J. Am. Chem. Soc.* **2003**, *125*, 16168–16169.
5. Mahan, G. D.; Gupta, R.; Xiong, Q. H.; Adu, C. K.; Eklund, P. C. Optical Phonons in Polar Semiconductor Nanowires. *Phys. Rev. B* **2003**, *68*, 073402.
6. Murray, C. B.; Norris, D. J.; Bawendi, M. G. Synthesis and Characterization of Nearly Monodisperse CdE (E = S, Se, Te) Semiconductor Nanocrystallites. *J. Am. Chem. Soc.* **1993**, *115*, 8706–8715.
7. Nirmal, M.; Dabbousi, B. O.; Bawendi, M. G.; Macklin, J. J.; Trautman, J. K.; Harris, T. D.; Brus, L. E. Fluorescence Intermittency in Single Cadmium Selenide Nanocrystals. *Nature* **1996**, *383*, 802–804.
8. Guichard, A. R.; Barsic, D. N.; Sharma, S.; Kamins, T. I.; Brongersma, M. L. Tunable Light Emission from Quantum-Confined Excitons in $TiSi_2$-Catalyzed Silicon Nanowires. *Nano Lett.* **2006**, *6*, 2140–2144.
9. Myalitsin, A.; Strelow, C.; Wang, Z.; Li, Z.; Kipp, T.; Mews, A. Diameter Scaling of the Optical Band Gap in Individual CdSe Nanowires. *ACS Nano* **2011**, *5*, 7920–7927.
10. D'Andrea, A.; Del Sole, R. Exciton Quantization and Polariton Propagation in Semiconductor Slabs: From Semi-infinite Crystals to Quantum Wells. *Phys. Rev. B* **1990**, *41*, 1413–1423.
11. Consadori, F.; Frindt, R. F. Crystal Size Effects on the Exciton Absorption Spectrum of WSe_2. *Phys. Rev. B* **1970**, *2*, 4893–4896.
12. Yan, Y.; Liao, Z.-M.; Bie, Y.-Q.; Wu, H.-C.; Zhou, Y.-B.; Fu, X.-W.; Yu, D.-P. Luminescence Blue-Shift of CdSe Nanowires beyond the Quantum Confinement Regime. *Appl. Phys. Lett.* **2011**, *99*, 103103.
13. Gudiksen, M. S.; Wang, J.; Lieber, C. M. Size-Dependent Photoluminescence from Single Indium Phosphide Nanowires. *J. Phys. Chem. B* **2002**, *106*, 4036–4039.
14. Chen, C.-W.; Chen, K.-H.; Shen, C.-H.; Ganguly, A.; Chen, L.-C.; Wu, J.-J.; Wen, H.-I.; Pong, W.-F. Anomalous Blueshift in Emission Spectra of ZnO Nanorods with Sizes beyond Quantum Confinement Regime. *Appl. Phys. Lett.* **2006**, *88*, 241905.
15. Yang, Y. H.; Chen, X. Y.; Feng, Y.; Yang, G. W. Physical Mechanism of Blue-Shift of UV Luminescence of a Single Pencil-Like ZnO Nanowire. *Nano Lett.* **2007**, *7*, 3879–3883.
16. Duan, X.; Huang, Y.; Agarwal, R.; Lieber, C. M. Single-Nanowire Electrically Driven Lasers. *Nature* **2003**, *421*, 241–245.
17. Chen, R.; Li, D.; Liu, B.; Peng, Z.; Gurzadyan, G. G.; Xiong, Q. H.; Sun, H. Optical and Excitonic Properties of Crystalline

ZnS Nanowires: Toward Efficient Ultraviolet Emission at Room Temperature. *Nano Lett.* **2010**, *10*, 4956–4961.
18. Zhang, Q.; Shan, X.-Y.; Feng, X.; Wang, C.-X.; Wang, Q.-Q.; Jia, J.-F.; Xue, Q.-K. Modulating Resonance Modes and Q Value of a CdS Nanowire Cavity by Single Ag Nanoparticles. *Nano Lett.* **2011**, *11*, 4270–4274.
19. Pan, A. L.; Liu, D.; Liu, R. B.; Wang, F. F.; Zhu, X.; Zou, B. S. Optical Waveguide through CdS Nanoribbons. *Small* **2005**, *1*, 980–983.
20. Bao, J.; Zimmler, M. A.; Capasso, F.; Wang, X.; Ren, Z. F. Broadband ZnO Single-Nanowire Light-Emitting Diode. *Nano Lett.* **2006**, *6*, 1719–1722.
21. Huang, Y.; Duan, X.; Lieber, C. M. Nanowires for Integrated Multicolor Nanophotonics. *Small* **2005**, *1*, 142–147.
22. Utama, M. I. B.; Zhang, J.; Chen, R.; Xu, X.; Li, D.; Sun, H.; Xiong, Q. H. Synthesis and Optical Properties of II-VI 1D Nanostructures. *Nanoscale* **2012**, *4*, 1422–1435.
23. Kind, H.; Yan, H.; Messer, B.; Law, M.; Yang, P. Nanowire Ultraviolet Photodetectors and Optical Switches. *Adv. Mater.* **2002**, *14*, 158–160.
24. Jie, J. S.; Zhang, W. J.; Jiang, Y.; Meng, X. M.; Li, Y. Q.; Lee, S. T. Photoconductive Characteristics of Single-Crystal CdS Nanoribbons. *Nano Lett.* **2006**, *6*, 1887–1892.
25. Singh, A.; Li, X.; Protasenko, V.; Galantai, G.; Kuno, M.; Xing, H.; Jena, D. Polarization-Sensitive Nanowire Photodetectors Based on Solution-Synthesized CdSe Quantum-Wire Solids. *Nano Lett.* **2007**, *7*, 2999–3006.
26. Bierman, M. J.; Lau, Y. K. A.; Kvit, A. V.; Schmitt, A. L.; Jin, S. Dislocation-Driven Nanowire Growth and Eshelby Twist. *Science* **2008**, *320*, 1060–1063.
27. Li, X.; Wang, X.; Xiong, Q. H.; Eklund, P. C. Mechanical Properties of ZnS Nanobelts. *Nano Lett.* **2005**, *5*, 1982–1986.
28. Xiong, Q. H.; Chen, G.; Acord, J. D.; Liu, X.; Zengel, J. J.; Gutierrez, H. R.; Redwing, J. M.; Lew Yan Voon, L. C.; Lassen, B.; Eklund, P. C. Optical Properties of Rectangular Cross-sectional ZnS Nanowires. *Nano Lett.* **2004**, *4*, 1663–1668.
29. Xiong, Q. H.; Wang, J.; Reese, O.; Lew Yan Voon, L. C.; Eklund, P. C. Raman Scattering from Surface Phonons in Rectangular Cross-sectional w-ZnS Nanowires. *Nano Lett.* **2004**, *4*, 1991–1996.
30. Rossler, U. *Landolt-Bornstein Numerical Data and Functional Relationships in Science and Technology, Group III: Condensed Matter. Semiconductors: II-VI and I-VII Compounds*, Vol. 41B; Springer: Berlin, 1999.
31. Agarwal, R.; Lieber, C. M. Semiconductor Nanowires: Optics and Optoelectronics. *Appl. Phys. A: Mater. Sci. Process.* **2006**, *85*, 209–215.
32. Li, Q. H.; Gao, T.; Wang, T. H. Optoelectronic Characteristics of Single CdS Nanobelts. *Appl. Phys. Lett.* **2005**, *86*, 193109.
33. Jiang, Y.; Zhang, W. J.; Jie, J. S.; Meng, X. M.; Fan, X.; Lee, S. T. Photoresponse Properties of CdSe Single-Nanoribbon Photodetectors. *Adv. Funct. Mater.* **2007**, *17*, 1795–1800.
34. Li, D. H.; Zhang, J.; Zhang, Q.; Xiong, Q. H. Electric Field-Dependent Photoconductivity in CdS Nanowires and Nanobelts: Exciton ionization, Franz-Keldysh and Stark Effects. Submitted to *Nano Lett*.
35. Greytak, A. B.; Barrelet, C. J.; Li, Y.; Lieber, C. M. Semiconductor Nanowire Laser and Nanowire Waveguide Electro-Optic Modulators. *Appl. Phys. Lett.* **2005**, *87*, 151103.
36. Xu, X.; Zhao, Y.; Sie, E. J.; Lu, Y.; Liu, B.; Ekahana, S. A.; Ju, X.; Jiang, Q.; Wang, J.; Sun, H.; *et al*. Dynamics of Bound Exciton Complexes in CdS Nanobelts. *ACS Nano* **2011**, *5*, 3660–3669.
37. Liu, B.; Chen, R.; Xu, X. L.; Li, D. H.; Zhao, Y. Y.; Shen, Z. X.; Xiong, Q. H.; Sun, H. D. Exciton-Related Photoluminescence and Lasing in CdS Nanobelts. *J. Phys. Chem. C* **2011**, *115*, 12826–12830.
38. Imada, A.; Ozaki, S.; Adachi, S. Photoreflectance Spectroscopy of Wurtzite CdS. *J. Appl. Phys.* **2002**, *92*, 1793–1798.
39. Voigt, J.; Spiegelberg, F. On the Dynamical Behaviour of Excitons in CdS Single Crystals. I. Correlation between Intrinsic Excitonic Absorption and Emission. *Phys. Status Solidi B* **1968**, *30*, 659–670.
40. Ullrich, B.; Schroeder, R.; Graupner, W.; Sakai, S. The Influence of Self-Absorption on the Photoluminescence of Thin Film CdS Demonstrated by Two-Photon Absorption. *Opt. Express* **2001**, *9*, 116–120.
41. Yoffe, A. D. Semiconductor Quantum Dots and Related Systems: Electronic, Optical, Luminescence and Related Properties of Low Dimensional Systems. *Adv. Phys.* **2001**, *50*, 1–208.
42. Yu, H.; Li, J.; Loomis, R. A.; Wang, L.-W.; Buhro, W. E. Two- versus Three-Dimensional Quantum Confinement in Indium Phosphide Wires and Dots. *Nat. Mater.* **2003**, *2*, 517–520.
43. Sumi, H. Exciton Luminescence at Low-Temperatures-Importance of Polariton Viewpoint. *J. Phys. Soc. Jpn.* **1976**, *41*, 526–535.
44. Burstein, E. Anomalous Optical Absorption Limit in InSb. *Phys. Rev.* **1954**, *93*, 632–633.
45. Rosencher, E.; Vinter, B. *Optoelectronics*; Cambridge University Press: New York, 2002.
46. Inaoka, T.; Nishida, A.; Hasegawa, M. Thickness Dependence of Carrier-Electron States in Doped Semiconductor Films. *J. Phys. Soc. Jpn.* **1999**, *68*, 4009–4013.
47. Hiruma, K.; Haraguchi, K.; Yazawa, M.; Madokoro, Y.; Katsuyama, T. Nanometre-Sized GaAs Wires Grown by Organo-Metallic Vapour-Phase Epitaxy. *Nanotechnology* **2006**, *17*, S369–S375.
48. Mohseni, P. K.; Rodrigues, A. D.; Galzerani, J. C.; Pusep, Y. A.; LaPierre, R. R. Structural and Optical Analysis of GaAsP/GaP Core-Shell Nanowires. *J. Appl. Phys.* **2009**, *106*, 124306.
49. An, J.; Xue, K.; Xie, W.; Li, Q.; Xu, J. Effects of an Oxygen Environment on the Electrical Properties of a Single CdS Nanobelt Device. *Nanotechnology* **2011**, *22*, 135702.
50. Yang, L. L.; Zhao, Q. X.; Israr, M. Q.; Sadaf, J. R.; Willander, M.; Pozina, G.; Yang, J. H. Indirect Optical Transition Due to Surface Band Bending in ZnO Nanotubes. *J. Appl. Phys.* **2010**, *108*, 103513.
51. Sze, S. M., Ng, K. K. *Physics of Semiconductor Devices*; Wiley: NJ, 2007.
52. Simpkins, B. S.; Mastro, M. A.; Eddy, J. C. R.; Pehrsson, P. E. Surface Depletion Effects in Semiconducting Nanowires. *J. Appl. Phys.* **2008**, *103*, 104313.
53. Galindo, A.; Pascual, P. *Quantum Mechanics I*; Spinger-Verlag: Berlin, 1990.
54. Jager, H.; Seipp, E. Burstein-Moss Shift in Heavily In-Doped Evaporated CdS Layers. *J. Appl. Phys.* **1981**, *52*, 425–427.
55. Liu, K. W.; Chen, R.; Xing, G. Z.; Wu, T.; Sun, H. D. Photoluminescence Characteristics of High Quality ZnO Nanowires and Its Enhancement by Polymer Covering. *Appl. Phys. Lett.* **2010**, *96*, 023111.
56. Utama, M. I. B.; Peng, Z.; Chen, R.; Peng, B.; Xu, X.; Dong, Y.; Wong, L. M.; Wang, S.; Sun, H.; Xiong, Q. H. Vertically Aligned Cadmium Chalcogenide Nanowire Arrays on Muscovite Mica: A Demonstration of Epitaxial Growth Strategy. *Nano Lett.* **2010**, *11*, 3051–3057.
57. Zhang, Q.; Zhang, J.; Utama, M. I. B.; Peng, B.; de la Mata, M.; Arbiol, J.; Xiong, Q. H. Exciton-Phonon Coupling in Individual ZnTe Nanorods Studied by Resonant Raman Spectroscopy. *Phys. Rev. B* **2012**, *85*, 085418.
58. Zhang, J.; Peng, Z.; Soni, A.; Zhao, Y.; Xiong, Y.; Peng, B.; Wang, J.; Dresselhaus, M. S.; Xiong, Q. H. Raman Spectroscopy of Few-Quintuple Layer Topological Insulator Bi_2Se_3 Nanoplatelets. *Nano Lett.* **2011**, *11*, 2407–2414.